P-ISSN 1991-8941
E-ISSN 2706-6703
Vol. 20, No. 1 (2026)

Journal of University of Anbar for Pure Science
(JUAPS)

journal homepage: juaps.uoanbar.edu.iq

Open Access

Original Paper

Evaluation the impact of temperature on the photodetection properties of V2O5/PANI nanocomposites

Tayba A. Ibrahim[1], **Obaid A.S.**[1,3*], **Ibraheem J Ibraheem**[2]

[1]Department of Physics, College of Science, University of Anbar, Ramadi, Iraq
[2]Department of Chemistry, College of Science, University of Anbar, Ramadi, Iraq
[3]Nanomaterials Research Center, University of Anbar, Ramadi, Iraq

ARTICLE INFO

Received: 27/06/2025
Accepted: 25/08/2025
Available online: 16/03/2026
April Issue
10.37652/juaps.2025.162061.1470

Cite @ JUAPS

Corresponding author
A.S.Obaid
sc.ahmed.s.obaid.alqayssei@uoanbar.edu.iq

ABSTRACT

V2O5/PANI nanocomposites were created using a hydrothermal method at 180 °C and 200 °C and then coated on p-type silicon substrates for photodetectors. The 180 °C sample showed better crystallinity with smaller crystals, more evenly distributed nanoparticles, and a more uniform surface than the 200 °C sample. FESEM and atomic force microscopy (AFM) analyses indicated enhanced surface homogeneity, distinct nanostructures, and improved charge-separation efficiency in the 180 °C sample. Raman spectra suggested better structural organization, while PL measurements revealed increased light-emission efficiency. The photodetectors were active in the 500–680 nm range, optimizing photodetection performance. The sample fabricated at 180 °C exhibited improved results compared to the one at 200 °C, with a photoresponse of 0.14 A/W, a detectivity of 1.58×10^{20} Jones, and an external quantum efficiency (EQE) of 55.41%. It also had a faster rise time and a steadier photoresponse, highlighting the importance of synthesis temperature in improving the structure and function of V2O5/PANI nanocomposite photodetectors.

Keywords: *Hybrid Photodetector, Hydrothermal, Nanocomposite, Temperature, V_2O_5/PANI*

1 INTRODUCTION

Photodetectors are essential components in today's widely used optoelectronic systems and devices. They convert incoming photons into electrical signals, enabling applications in security, medical diagnoses, and environmental monitoring [1, 2]. Developing highly responsive photodetectors that respond rapidly and remain stable over long periods under varied operating conditions remains challenging for practical applications. Current studies suggest that nanostructured materials can further improve photodetector performance; their large surface area and tunable features are often key to this improvement [3–5]. Hybrid organic–inorganic nanostructured composites have been developed as one of the most appropriate approaches, combining the mechanical flexibility, processability, and tunable optoelectronic properties of polymers with the high carrier mobility, stability, and light-absorption properties of inorganic semiconductors [6]. Vanadium pentoxide (V2O5) has high chemical flexibility, a low bandgap (2.2–2.8 eV), good visible-light absorption, and thermal stability, making it an attractive inorganic material [7,8]. However, the poor intrinsic conductivity of pure V2O5 and its slow charge-transport kinetics restrict its independent application in high-speed photodetectors. To overcome these obstacles, V2O5 has been combined with conductive polymers such as polyaniline (PANI) to create nanocomposites that leverage the complementary qualities of both components. PANI is an excellent option for hybridization because of its high electrical conductivity, outstanding environmental stability, and ease of synthesis [9, 10]. Under typical conditions, the V2O5/PANI nanocomposite structure provides enhanced

light–matter interaction, fewer recombination centers, and improved carrier-transport pathways, thereby increasing overall photodetector performance. Although significant advancements have been made in this field, the performance of photodetectors based on nanocomposite technology remains adversely affected by temperature and other environmental factors. Temperature variation affects responsivity, detectivity, and device linearity, as well as fundamental processes such as carrier mobility, generation–recombination rates, trap-state dynamics, and material morphology [11]. Thermal effects can be both beneficial and detrimental to device performance, depending on the material system and operational range. This thermal response must be considered when these nanocomposite systems are applied in practice because they experience temperature fluctuations during operation. A recent study reported that hybrid nanocomposites, such as a low-temperature in situ-synthesized reduced graphene oxide (rGO)/ZnO structure, can exhibit significantly enhanced photodetection sensitivity. Connecticut, which results from improved carrier transport and lower trap-assisted recombination, particularly under different thermal conditions [12]. These findings highlight the importance of nanoscale material engineering in creating thermally stable, high-performance photodetectors. Similarly, Khan et al. investigated the photodetector capabilities of PANI/CuO nanostructures prepared via hydrothermal methods and found that temperature is critical in modifying their photoresponse behavior [13]. Their findings showed that moderate thermal activation improves charge separation and transport; however, excessive heating can trigger degradation processes that limit device performance. These observations underscore the need to carefully manage temperature conditions while optimizing photodetector functionality in polymer–inorganic hybrid systems. Overall, the results highlight the intricate relationship between material stability and thermal activation that governs photodetector performance. V2O5/PANI nanocomposites demonstrate a unique amalgamation of elevated thermal stability and improved electrical conductivity; however, the influence of temperature fluctuations on their optoelectronic performance is still inadequately comprehended. This work examines the temperature-dependent characteristics of V2O5/PANI-based photodetectors, concentrating on critical metrics such as responsivity, response time, and photo gain. The objective is to achieve a deeper understanding of charge-transport mechanisms and to facilitate the systematic design of advanced photodetectors with enhanced thermal adaptability and efficiency.

2 MATERIALS AND METHODS

2.1 Synthesis of V_2O_5/PANI nanocomposites

The V2O5/PANI nanocomposite was prepared via a hydrothermal process, known for its ease of use, low cost, and being free of hazardous chemicals or surfactants. V_2O_5 powder (0.125 g) and polyaniline (PANI) (0.25 g) were dispersed in 25 mL of deionized water and briefly ultrasonically agitated to ensure homogeneity. The resulting suspension was hydrothermally treated at two distinct temperatures (180 °C and 200 °C) in a stainless-steel autoclave lined with Teflon for six hours. The temperature environment promoted strong interfacial contact between V_2O_5 and PANI, encouraging the formation of a hybrid nanostructure with potential charge-transfer synergy.

2.2 Fabrication of V_2O_5/PANI photodetector

The V2O5/PANI nanocomposite was applied to p-type silicon substrates to fabricate the device using a spray-coating method. The substrates were preheated on a hot plate set to 80-85 °C to ensure good adhesion and a uniform coating. A spraying nozzle was positioned 35 cm above the substrate and contained 10 mL of the V_2O_5/PANI dispersion. Fifty spray cycles were used, with a 5-second spray burst followed by a 25-second drying time between cycles. This technique enabled controlled deposition of thin films with adjustable thickness based on spray concentration and duration. Finally, to complete the photodetector device design, silver (Ag) electrodes were applied by drop casting, as shown in Figure 1.

2.3 Characteristics

An X-ray diffractometer (SHIMADZU, 6000) was used to analyze the V_2O_5/PANI layer using CuKα radiation. Meanwhile, morphological examinations were recorded using field-emission scanning electron microscopy (Hitachi). Using an AFM, the nanoparticles' topography, surface morphology, and particle size distribution were examined (Mountains SPIP Expert 8.2.9621). The optical behavior was studied using the FS-1401004 instrument, which measured photoluminescence within a scanning range of 330 to 800 nm with an excitation wavelength of 330 nm. To analyze the bonding structure, a (SUNSHINE-V2-86) device was used to measure the Raman spectrum. Using a Keithley 237 SMU and a tungsten-halogen light, the current–voltage (I–V) behavior was investigated in both bright and dark conditions.

Using a monochromatic setup, the spectral response of the artificial visible-light V_2O_5/PANI photodetector on a silicon substrate was continuously measured over a wide wavelength range at an illumination power of 10 mW/cm2.

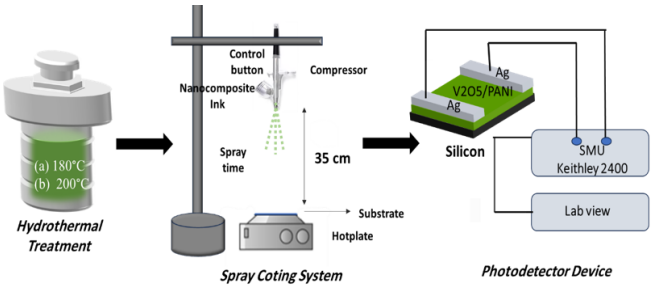

Fig. 1 Diagrammatic representation of the V2O5/PANI-based photodetector device's synthesis and manufacturing process

3 RESULTS AND DISCUSSION

3.1 Characterization of the prepared photoactive layer

As shown in Figure 2 and Table 1, the X-ray diffraction (XRD) patterns of thermally treated V2O5/PANI thin films at 180 °C showed noticeable crystalline peaks at 2θ = 20.12°, 26.9°, and 31.1°. According to the JCPDS card no. 00-009-03877, these correspond to the (001), (110), and (400) planes of orthorhombic V2O5, respectively [14]. These peaks validate the development of a stratified crystalline structure, which is essential for anisotropic conductivity and effective ion transport. Minor reflections at $2\theta \approx 8.38°$ and 38.13° were ascribed to the (100) and (401) planes of monoclinic VO2, signifying the existence of partly reduced vanadium oxide (V4+ states) [15]. A distinct peak at 2θ = 23.16° was observed, indicative of the semi-crystalline arrangement of PANI chains, whereas a low-angle peak at around 9.25° signified the existence of emeraldine salt-type PANI [16].

Significant structural alterations were detected when the thermal treatment temperature was elevated to 200 °C. The crystallite sizes of V_2O_5 in the (110) and (400) planes increased from 53.04 nm to 111.58 nm and from 19.17 nm to 32.94 nm, respectively, indicating enhanced crystallinity with increasing temperature. Simultaneously, microstrain and defect density increased in the VO2 phase while decreasing in V_2O_5, indicating structural instability in VO2 and improved ordering in V2O5. The vanishing of the (401) peak of VO2 and the formation of a new peak at 2θ = 15.43°, attributed to the (200) plane of the intermediate V6O13 phase, further substantiated a temperature-induced phase transition [17]. The mixed-valence phase (V5+/V4+) generally arises after partial reduction or solid-state transition of V_2O_5. Moreover, shifts in the positions of V_2O_5 peaks, namely (001) and (110), suggested potential lattice relaxation or differences in interlayer spacing resulting from thermal strain or interaction with the PANI matrix [18].

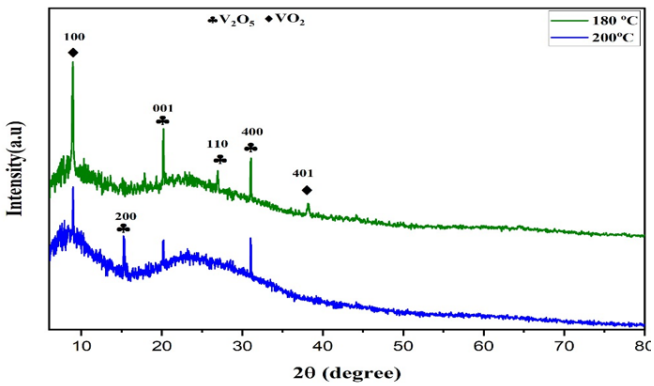

Fig. 2 The XRD patterns of V_2O_5/PANI nanocomposites at 180°C and 200°C demonstrate phase and crystallinity variations that depend on temperature

Table 1 XRD analysis determined the crystallographic characteristics of V_2O_5/PANI nanocomposites at 180 and 200°C.

Code Sample	2θ	FWHM	Miller ndices	Crystalline size(nm)	Dislocation density(δ) $\times 10^{-3}$	Micro strains (nm^{-2}) $\times 10^{-3}$	Crystal system	Chemical formula
180	8.38	0.07	100	113.79	0.077	4.2	Monoclinic	VO_2
	20.12	0.307	001	26.28	1.44	7.55	Orthorhombic	V_2O_5
	26.9	0.154	110	53.04	0.35	2.80	Orthorhombic	V_2O_5
	31.09	0.43	400	19.17	2.72	6.74	Orthorhombic	V_2O_5
	38.13	0.093	401	90.379	0.122	1.17	Monoclinic	VO_2
200	8.2	0.29	100	61.29	1.32	17.65	Monoclinic	VO_2
	15.43	0.07	200	114.4	0.08	2.26	Orthorhombic	V_6O_{13}
	20.17	0.123	110	65.46	0.233	3.013	Orthorhombic	V_2O_5
	31.7	0.25	400	32.94	0.92	3.84	Orthorhombic	V_2O_5

The morphological characteristics of V2O5/PANI nanocomposites synthesized at 180 °C and 200 °C were analyzed using FESEM, revealing a significant effect of hydrothermal temperature on the nanostructure. Figure 3 illustrates that the sample synthesized at 180 °C (a) displayed evenly dispersed spherical nanoparticles within a nanofibrous PANI matrix. This configuration provides an extensive surface area and multiple active sites, promoting effective charge separation and transport at the metal oxide/polymer interface. Conversely, at 200 °C (b), the images revealed increased particle growth and significant agglomeration, attributable to accelerated grain-growth kinetics at elevated temperatures. Although

this may enhance interparticle interaction, it reduces the effective surface area and may impede photodetector performance [19]. Furthermore, the morphology of the PANI component is significantly altered at higher synthesis temperatures. According to earlier research, higher temperatures result in more compact granular or porous agglomerates, whereas lower temperatures promote the formation of fibrous or tubular structures [20]. These structural differences directly influence the electrical and optical properties of the nanocomposite, with porous, interconnected networks under optimal thermal conditions enhancing charge mobility and interfacial integration with metal oxides.

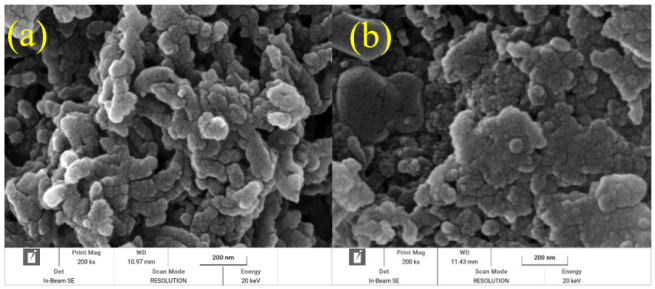

Fig. 3 FESEM images of V_2O_5/PANI nanocomposites produced at (a) 180°C and (b) 200°C hydrothermal temperatures at 6 hours demonstrate how temperature affects particle aggregation and surface shape

Figure 4 shows 3D AFM images of the V2O5/PANI nanocomposite, highlighting how hydrothermal treatment temperature affects surface morphology. At 180 °C, the sample displayed a relatively homogeneous surface with evenly dispersed nanoparticles and moderate roughness, facilitating effective photon trapping and charge production [21]. Conversely, at 200 °C, the surface exhibited increased roughness, notable nanostructured protrusions, and a more intricate topology, signifying heterogeneous material buildup that may impede charge transfer and elevate surface recombination rates [22]. These findings underscore the importance of temperature regulation in optimizing nanoscale surface characteristics to improve photodetector efficacy [23].

Figure 5 displays the Raman spectra of the thermally produced V2O5/PANI nanocomposite at two distinct temperatures, 180 °C and 200 °C. The spectra show distinct vibrational signatures indicating structural and chemical interactions among the composite components at different temperatures.

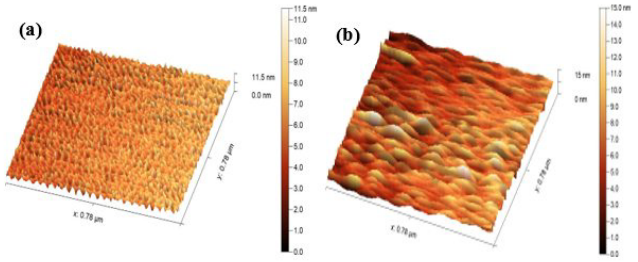

Fig. 4 AFM 3-D images and particle size histograms behavior of V_2O_5/PANI nanocomposites subjected to hydrothermal treatment at 180°C and 200°C

Significant peaks are identified at 148, 308, 360, 512, 590, 695, 780, and 940 cm^{-1}, corresponding to the orthorhombic phase of V2O5. The low-frequency peaks (<400 cm^{-1}) relate to lattice vibrations and bending modes of V–O–V linkages, whereas the bands between 500 and 700 cm^{-1} are linked to in-plane vibrational modes of the V–O network in the layered oxide structure [24]. The prominent band at 940 cm^{-1} is attributed to terminal V=O stretching vibrations, frequently regarded as a marker of crystallinity and the presence of symmetric terminal bonds [25].

Additional peaks at 470, 775, 870, 1200, 1262, 1321, 1502, and 1569 cm^{-1} indicate the molecular structure of polyaniline (PANI) in its emeraldine salt configuration. Peaks in the 440–870 cm^{-1} range arise from C–H vibrations and C–N–C bending [26], whereas the bands between 1200 and 1321 cm^{-1} are ascribed to C–N and C=N stretching, sometimes linked to polaronic charge carriers [9, 27]. The prominent peaks at 1480–1569 cm^{-1} indicate C=C stretching within the aromatic rings, reflecting the polymer oxidation state and intrachain conductivity [28].

Comparing the spectra obtained at 180 °C and 200 °C reveals small but significant variations in peak intensity and width, reflecting changes in the vibrational environment induced by thermal processing. A slight reduction in the intensity of the 940 cm^{-1} (V=O) peak is noted at 200 °C, suggesting reduced symmetry or increased distortion of the terminal oxygen bonds due to polymer interaction. Simultaneously, the PANI-related peaks, especially at 1321 and 1502 cm^{-1}, show increased intensity and broadening at elevated temperatures, indicating greater amorphous character and thermally induced rearrangement within the polymer chains. Furthermore, subtle spectral alterations in the 700–800 cm^{-1} range indicate partial reduction of V5+ to V4+, presumably aided

by the –NH– groups of PANI, suggesting the potential development of VO2-like domains or the formation of new V–N chemical bonds within the hybrid structure [29]. These vibrational changes indicate that increasing the synthesis temperature modifies the composite's internal bonding and molecular arrangement, affecting both the oxide framework and polymer matrix, as evidenced by the Raman response.

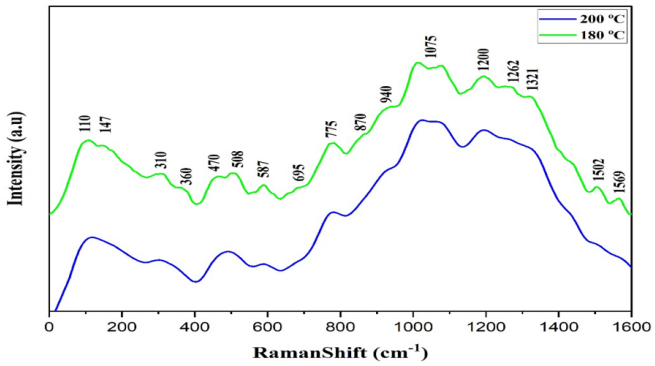

Fig. 5 The Raman spectra of V_2O_5/PANI nanocomposites synthesized at 180°C and 200°C, showing vibrational mode assignments and structural variations

The PL spectra of V2O5/PANI nanocomposites synthesized at 180 °C and 200 °C reveal significant variations in emission intensity and band positions, indicating that the optical properties are strongly influenced by the hydrothermal synthesis temperature. Defect states, band-to-band transitions, and recombination kinetics of the nanocomposites are reflected by the emission peaks. Figure 6 shows that, at 180 °C, the spectrum exhibits a dominant violet emission peak at 364 nm, which is ascribed to $\pi \rightarrow \pi^*$ transitions in the benzenoid units of PANI [30]. Emission peaks at 433 and 443 nm are attributed to band-to-band transitions in V2O5 [31]. The 550 and 570 nm peaks in both samples correspond to electron transitions from the valence band of V2O5 to the π orbital of the emeraldine salt of PANI [32, 33]. Emission bands at 704 and 716 nm were also observed and are associated with transitions via deep-level defect states due to oxygen vacancies or lattice distortions generated by extended heat treatment; these faint peaks were observed concurrently with the removal of the dipole excitation [34]. The stronger emission intensities at 200 °C indicate a higher density of localized states and defects, which promotes enhanced radiative recombination. The reduced emission intensity at 180 °C is consistent with the FESEM and XRD data and suggests better crystallinity and fewer defect centers. Furthermore, the minor redshift observed in the emission bands can be attributed to bandgap narrowing caused by increased interfacial contact and orbital overlap between PANI chains and V2O5 nanostructures. This electronic connection modulates charge-carrier dynamics and can enable more efficient charge separation, benefiting optical devices such as solar cells and photodetectors [35].

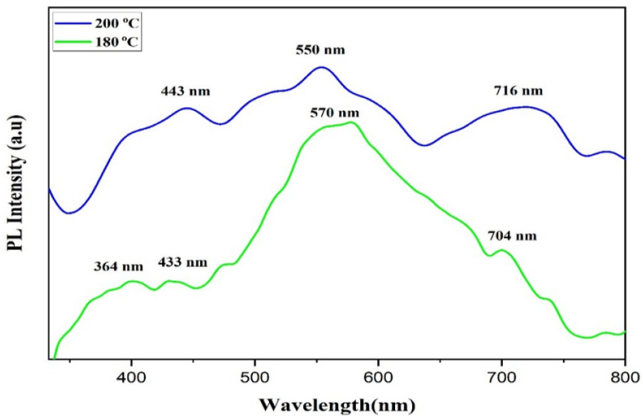

Fig. 6 Illustrates the PL spectra of V_2O_5/PANI nanocomposites synthesized at 180°C and 200°C

Figure 7 depicts the I–V characteristics of V2O5/PANI nanocomposite photodetectors subjected to heat treatment at 180 °C and 200 °C for 6 hours. Under forward bias (+5 V), the device treated at 180 °C exhibited a photocurrent of 3543.4 µA and a dark current of 895.25 µA. Moreover, under reverse bias (-5 V), the photocurrent reached 1236.4 µA, and the dark current measured 339.1 µA. Conversely, the sample treated at 200 °C exhibited a photocurrent of 2112.7 µA and a dark current of 570.8 µA at +5 V, and 912.9 µA (photocurrent) compared to 207.2 µA (dark current) at -5 V. The notable improvement in photoresponse at 180 °C is ascribed to the formation of a more effective internal n–p heterojunction between V2O5 (n-type) and PANI (p-type), which facilitates a stronger built-in electric field and improved separation of photogenerated charge carriers [36]. The substantial forward photocurrent (3543.4 µA) suggests elevated carrier mobility and reduced recombination, whereas the lower dark current (895.25 µA) indicates inhibited thermally induced charge leakage. The higher reverse photocurrent (1236.4 µA) further substantiates that the built-in field facilitates carrier extraction despite the applied bias, indicating an effective self-powered photodetector.

The decreased photocurrent in the sample treated at

200 °C is associated with the emergence of the V6O13 phase, which generates trap states inside the bandgap owing to its mixed valence (V4+/V5+). These traps act as recombination centers, reducing the lifetimes and mobilities of photoexcited carriers [17]. The increased surface roughness detected by AFM in this sample disrupts the internal field homogeneity and creates carrier-scattering sites, resulting in a significant reduction in total photoresponse. The dark currents in both samples were lower than their corresponding photocurrents, indicating photoinduced carrier generation; nevertheless, the elevated dark current at 200 °C implies an increase in intrinsic defects and diminished barrier effectiveness at the heterojunction interface. Overall, the comparative current values indicate that the sample treated at 180 °C demonstrates higher optoelectronic performance, characterized by improved light-to-current conversion efficiency and enhanced carrier dynamics at the heterojunction interface.

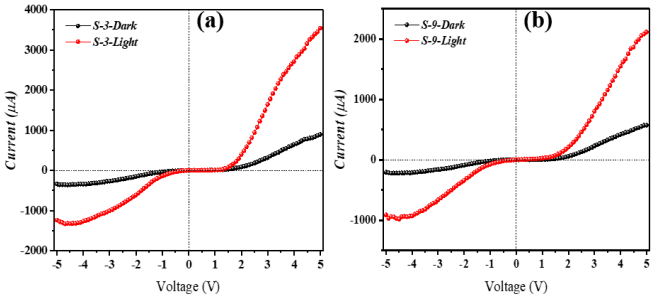

Fig. 7 Current -voltage (I-V) characteristics of V_2O_5 /PANI photodetectors synthesized at 180°C and 200°C under dark and illuminated conditions

Figure 8 displays the time-dependent photocurrent responses of V2O5/PANI nanocomposite photodetectors fabricated at 180 °C and 200 °C under multiple 10 mW/cm2 illumination power cycles over three 10 s pulse switching cycles at 2 bias voltages. The devices exhibit steady, repeatable photoresponse under periodic illumination. The key statistics derived from these observations are the rise time (τrise), defined as the time required for the current to increase from 10% to 90% of its peak value after the light is turned on, and the decay time (τfall), defined as the time required for the current to decrease from 90% to 10% after the light is turned off [37].

The differences in photo-response dynamics of V2O5/PANI-based photodetectors annealed at 180 °C and 200 °C are mainly due to structural and morphological changes induced by the different annealing temperatures. At 180 °C, moderate thermal energy promotes partial reorganization of polymer chains, enhances interfacial bonding, and regulates the crystallization of V2O5 nanostructures, thereby reducing trap densities and enabling effective exciton dissociation. Thus, the device demonstrates a rapid response time of 0.62 seconds and a short recovery time of 0.59 seconds, indicating efficient charge separation and limited recombination pathways [38, 39]. Conversely, annealing at 200 °C facilitates excessive crystal growth, partial disintegration of the PANI matrix, and the emergence of grain boundaries and inhomogeneous surfaces, introducing deep trap states and electronic disorder. These characteristics impede the transport of photogenerated carriers, resulting in an extended response time of 1.29 seconds. However, the recovery time remains relatively constant at 0.58 seconds, suggesting that carrier recombination dynamics are not markedly modified [40].

Furthermore, the higher annealing temperature of 200 °C results in increased surface roughness, an augmented proportion of amorphous regions within the polymer matrix, and the formation of intermediate phases such as V6O13 [41]. These structural modifications create trap centers and scattering sites, negatively impacting carrier mobility and delaying the device's light responsiveness. The consistent recovery time suggests a dynamic equilibrium between enhanced trapping and stable recombination under these conditions [42]. From a quantum-physics standpoint, these behaviors are fundamentally affected by parameters such as exciton lifetime, carrier hopping time, and the density of states near the band edges. Deep trap levels and lattice disorder reduce the activation energy for carrier release and affect transition rates between excited and ground states, thereby regulating the photodetector's response and recovery characteristics. Recent investigations confirm that mild annealing boosts interfacial order and device performance, whereas overheating deteriorates heterojunction quality and increases non-radiative losses [43, 44].

Figure 9 and Table 2 show the results of a thorough evaluation of the optical performance of V2O5/PANI photodetectors synthesized at 180 °C and 200 °C using photoresponsivity (R) (the ratio of a visible photodetector's output photocurrent to illumination power, R = I_Ph/P_i), specific detectivity (D^*), with the relation $(R_\lambda/\sqrt{2qI_D})$, where I_D is the dark current and q is the electron charge.

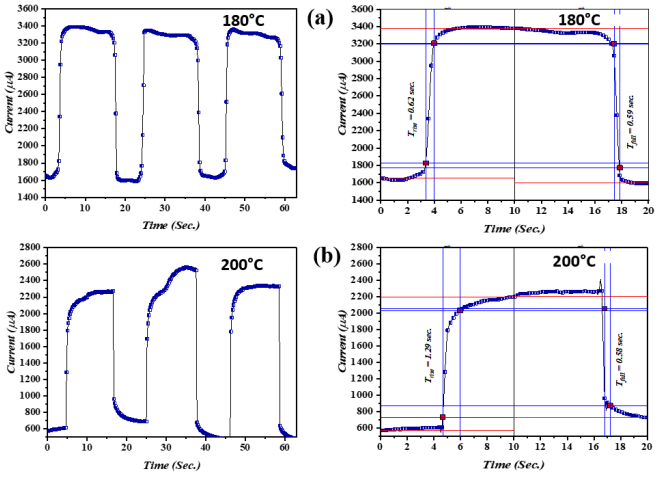

Fig. 8 Time-dependent photo-response behavior of V_2O_5/PANI photodetectors synthesized at (a) 180°C and (b) 200°C under periodic light on/off illumination

External quantum efficiency (EQE) is related to R using the formula (EQE = 1240 × R/λ× 100%), where λ is the wavelength [45–47]. The visible range (400–700 nm) showed prominent peaks in photoresponsivity, which measures the photocurrent produced per unit of incident light. The sample fabricated at 180 °C exhibited much higher R values, especially at 520 nm. The optimal synthesis temperature promotes more effective carrier separation and inhibits recombination, resulting in increased interfacial charge transfer between the oxide and the polymer matrix and decreased trap states [48].

The 180 °C sample showed better detectivity, especially in the mid-visible range, where its D* values were noticeably higher than those of the 200 °C sample. This improvement is probably due to improved morphology, enhanced interfacial coupling, and reduced dark current at 180 °C, which lower noise levels and enable more successful detection of weak light signals [49]. External quantum efficiency (EQE), which reflects the fraction of absorbed photons converted into carriers, showed a similar pattern.

Over the entire spectrum, the 180 °C device consistently showed higher EQE values, indicating that a greater percentage of photons contributed to carrier generation and collection in this sample [50].

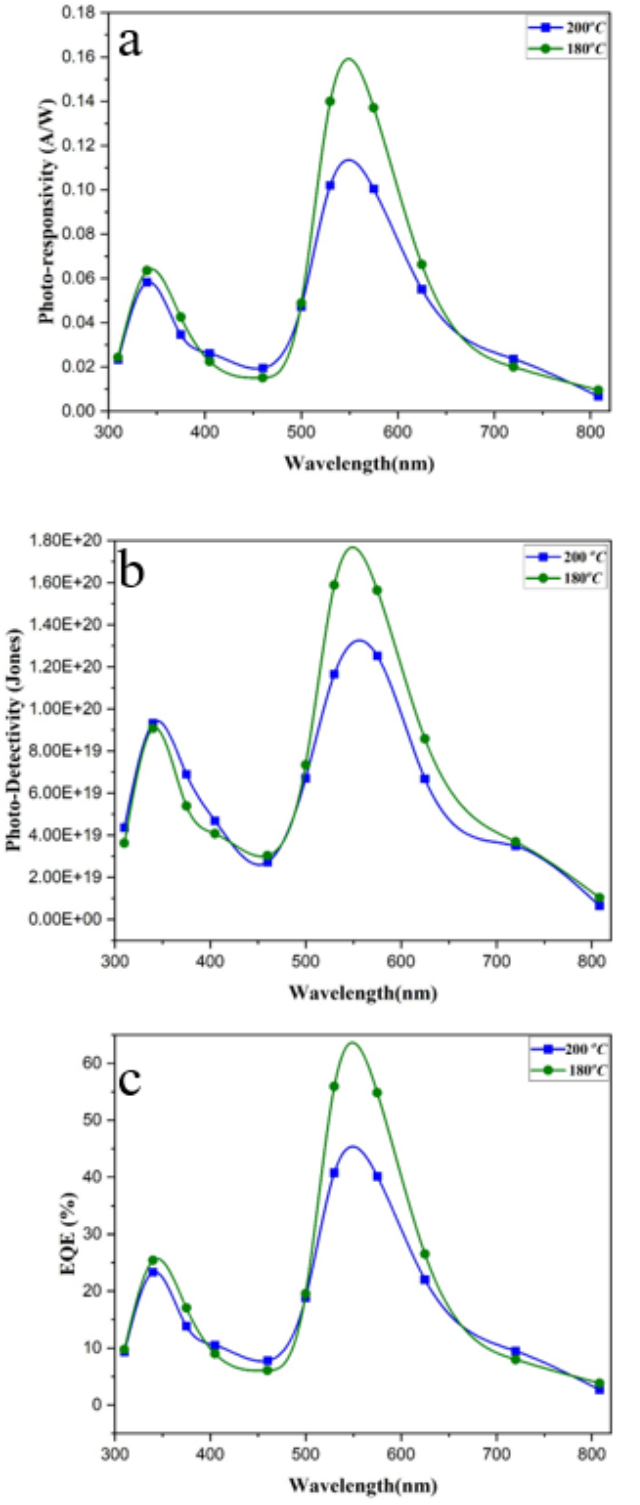

Fig. 9 Comparative V_2O_5/PANI photodetectors synthesized at 180°C and 200°C in terms of (a)Photoresponsivity,(b) Detectivity, and (c)External Quantum Efficiency (EQE)

Table 2 Merits comparing the performance of the V_2O_5/PANI heterojunction photodetector

Parameter	**180**°C	**200**°C
Forward Light Current(μA)	3543.4	2112.7
Reverse Light Current (μA)	1300.4	912.9
Forward dark Current (μA)	895.25	570.8
Reverse Dark Current (μA)	339.1	207.2
Photoresponsivity (R) A/W	0.14	0.11
Detectivity (D) $\times 10^{20}$Jones	1.58	1.24
External Quantum Efficiency (EQE %)	55.41	41.07

The improvements observed in the 180 °C sample's R, D^*, and EQE characteristics underscore the importance of the synthesis temperature for optimizing photodetector performance. Specifically, at this temperature, the enhanced microstructure, stronger interfacial bonding, and better polymer penetration contribute to faster carrier dynamics and lower recombination rates, ultimately boosting quantum efficiency and photoconductive responsiveness [51].

4 CONCLUSION

This work synthesizes V2O5/PANI nanocomposites using a surfactant-free hydrothermal technique at 180 °C and 200 °C. The structural, optical, morphological, and optoelectronic characteristics were examined comprehensively. V2O5/PANI nanocomposites produced at 180 °C exhibited better morphological, structural, and optoelectronic properties than those synthesized at 200 °C. XRD assessment showed sharper peaks at 180 °C, indicating greater crystallinity and lower lattice strain. FESEM images demonstrated a more uniform dispersion of V2O5 within the PANI matrix. At 180 °C, PL spectroscopy indicated reduced defect-related recombination, whereas Raman analysis suggested stronger interactions between polymer chains and metal oxide phases. Electrical and photo-response experiments confirmed that the 180 °C-based photodetector exhibited a higher photocurrent, a faster rise time, and a slightly slower decay, indicating efficient carrier generation and extended carrier separation. This sample achieved a responsivity of 0.14 A/W, a detectivity of 1.58×10^{11} Jones, and an EQE of 55.41%, indicating that 180 °C is the optimal synthesis temperature for high-efficiency photodetection applications.

Acknowledgement

N/A

Funding source

No funds received.

Data availability

N/A

DECLARATIONS

Conflict of interest

The authors declare that they have no conflict of interest.

Consent to publish

N/A

Ethical approval

N/A

REFERENCES

[1] Konstantatos G. Current status and technological prospect of photodetectors based on two-dimensional materials. Nature Communications. 2018;9(1). 10.1038/s41467-018-07643-7

[2] Gundepudi K, Neelamraju PM, Sangaraju S, Dalapati GK, Ball WB, Ghosh S, et al. A review on the role of nanotechnology in the development of near-infrared photodetectors: materials, performance metrics, and potential applications. Journal of Materials Science. 2023;58(35):13889–13924. 10.1007/s10853-023-08876-8

[3] VJ L, Oh J, Nayak AP, Katzenmeyer AM, Gilchrist KH, Grego S, et al. A Perspective on Nanowire Photodetectors: Current Status, Future Challenges, and Opportunities. IEEE Journal of Selected Topics in Quantum Electronics. 2011;17(4):1002–1032. 10.1109/jstqe.2010.2093508

[4] Fan Z, Lu JG. Gate-reshable nanowire chemical sensors. Applied Physics Letters. 2005;86(12). 10.1063/1.1883715

[5] Mahdi MM, Salim ET, Obaid AS. Single Step Formation Of Gold Core -Niobium Pentoxide Shell Nanoparticles Using Laser Ablation Technique: Effect of Laser Pulse Number. International Journal of Nanoelectronics and Materials (IJNeaM). 2025;18(June):125–138. 10.58915/ijneam.v18ijune.2337

[6] Zhang S, Geryak R, Geldmeier J, Kim S, Tsukruk VV. Synthesis, Assembly, and Applications of Hybrid Nanostructures for Biosensing. Chemical Reviews. 2017;117(20):12942–13038. 10.1021/acs.chemrev.7b00088

[7] Assem FL, Levy LS. A Review of Current Toxicological Concerns on Vanadium Pentoxide and Other Vanadium Compounds: Gaps in Knowledge and Directions for Future Research. Journal of Toxicology and Environmental Health, Part B. 2009;12(4):289–306. 10.1080/10937400903094166

[8] Altowyan AS, Hakami J, Algarni H, Shkir M. Enhancing the optoelectronic properties of V2O5 thin films through Tb doping for photodetector applications. Journal of Alloys and Compounds. 2023;960:170911. 10.1016/j.jallcom.2023.170911

[9] Stejskal J, Gilbert RG. Polyaniline. Preparation of a conducting polymer(IUPAC Technical Report). Pure and Applied Chemistry. 2002;74(5):857–867. 10.1351/pac200274050857

[10] Kumar H, Boora A, Yadav A, Rajni, Rahul. Polyaniline-metal oxide-nano-composite as a nano-electronics, opto-electronics, heat resistance and anticorrosive material. Results in Chemistry. 2020;2:100046. 10.1016/j.rechem.2020.100046

[11] Rahman S, Azharuddin M, Bansal J, Bilal M, Tabassum R, Hafiz AK. Role of temperature on CdS and MoS2 doped SnO2 nanostructures: Potential applications in photodetection and temperature dependent current-voltage characteristics. Journal of Alloys and Compounds. 2023;941:168901. 10.1016/j.jallcom.2023.168901

[12] Liu S, Li B, Kan H, Liu H, Xie B, Zhu X, et al. Low temperature in-situ preparation of reduced graphene oxide/ZnO nanocomposites for highly sensitive photodetectors. Journal of Materials Science: Materials in Electronics. 2017;28(13):9403–9409. 10.1007/s10854-017-6681-4

[13] Ahmed MS, Iftikhar MA, Nabeel AB. Photodetector properties of polyaniline/cuo nanostructures synthesized by hydrothermal technique. 2019

[14] Shafeeq KM, Athira VP, Kishor CHR, Aneesh PM. Structural and optical properties of V2O5 nanostructures grown by thermal decomposition technique. Applied Physics A. 2020;126(8). 10.1007/s00339-020-03770-5

[15] Kundu S, Satpati B, Kar T, Pradhan SK. Microstructure characterization of hydrothermally synthesized PANI/V2O5·nH2O heterojunction photocatalyst for visible light induced photodegradation of organic pollutants and non-absorbing colorless molecules. Journal of Hazardous Materials. 2017;339:161–173. 10.1016/j.jhazmat.2017.06.034

[16] Sydulu Singu B, Srinivasan P, Pabba S. Benzoyl Peroxide Oxidation Route to Nano Form Polyaniline Salt Containing Dual Dopants for Pseudocapacitor. Journal of The Electrochemical Society. 2011;159(1):A6–A13. 10.1149/2.036201jes

[17] Mutta GR, Popuri SR, Ruterana P, Buckman J. Single step hydrothermal synthesis of mixed valent V 6 O 13 nano-architectures: A case study of the possible applications in electrochemical energy conversion. Journal of Alloys and Compounds. 2017;706:562–567. 10.1016/j.jallcom.2017.02.272

[18] Sharma N, Singh A, Kumar N, Tiwari A, Lal M, Arya S. A review on polyaniline and its composites: from synthesis to properties and progressive applications. Journal of Materials Science. 2024;59(15):6206–6244. 10.1007/s10853-024-09562-z

[19] Jalil MA, Khan MNI, Mandal S, Chowdhury FUZ, Hossain MM, Jana D, et al.. Impact of reaction temperatures on the particle size of V2O5 synthesized by facile hydrothermal technique and their auspicious photocatalytic performance in dye degradation. arXiv; 2022. 10.48550/ARXIV.2205.04046

[20] Moyseowicz A, Gryglewicz G. Hydrothermal-assisted synthesis of a porous polyaniline/reduced graphene oxide composite as a high-performance electrode material for supercapacitors. Composites Part B: Engineering. 2019;159:4–12. 10.1016/j.compositesb.2018.09.069

[21] Li J, Li X, Zeng L, Fan S, Zhang M, Sun W, et al. Functionalized nitrogen-doped carbon dot-modified yolk–shell ZnFe2O4 nanospheres with highly efficient light harvesting and superior catalytic activity. Nanoscale. 2019;11(9):3877–3887. 10.1039/c8nr08611g

[22] Yang D, Jang JG, Lim J, Lee Jk, Kim SH, Hong JI. Correlations of Optical Absorption, Charge Trapping, and Surface Roughness of TiO2Photoanode Layer Loaded with Neat Ag-NPs for Efficient Perovskite Solar Cells. ACS Applied Materials & Interfaces. 2016;8(33):21522–21530. 10.1021/acsami.6b07079

[23] Mahdi MM, Salim ET, Obaid AS. Au@Nb2O5 core/porous-shell nanoparticles: Synthesis and characterization at different laser pulse. Materials Today Communications. 2025;46:112719. 10.1016/j.mtcomm.2025.112719

[24] Frost RL, Palmer SJ, Čejka J, Sejkora J, Plášil J, Bahfenne S, et al. A Raman spectroscopic study of the different vanadate groups in solid-state compounds—model case: mineral phases vésigniéite [BaCu3(VO4)2(OH)2] and volborthite [Cu3V2O7(OH)2·2H2O]. Journal of Raman Spectroscopy. 2011;42(8):1701–1710. 10.1002/jrs.2906

[25] M T, S P, Ranganatha V L, Al-Tamimi J, Al-Odayni AB, H B VP, et al. Facile and green-assisted synthesis of V2O5 Nps and investigated their multifunctional activities. Ionics. 2024;30(12):8687–8701. 10.1007/s11581-024-05862-1

[26] Krysa M, Szymańska-Chargot M, Zdunek A. FT-IR and FT-Raman fingerprints of flavonoids – A review. Food Chemistry. 2022;393:133430. 10.1016/j.foodchem.2022.133430

[27] Synytsya A, Janstová D, Šmidová M, Synytsya A, Petrtýl J. Evaluation of IR and Raman spectroscopic markers of human collagens: Insides for indicating colorectal carcinogenesis. Spectrochimica Acta Part A: Molecular and Biomolecular Spectroscopy. 2023;296:122664. 10.1016/j.saa.2023.122664

[28] Turkten N, Karatas Y, Uyguner-Demirel CS, Bekbolet M. Preparation of PANI modified TiO2 and characterization under pre- and post- photocatalytic conditions. Environmental Science and Pollution Research. 2023;30(51):111182–111207. 10.1007/s11356-023-30090-x

[29] Navas D. In: Morphology and Oxidation State Transitions under Hydrothermal Treatment on Vanadium Oxide (V) Systems. B P International; 2024. p. 1–65. 10.9734/bpi/cicms/v5/7562a

[30] Banerjee S, Sarmah S, Kumar A. Photoluminescence studies in HCl-doped polyaniline nanofibers. Journal of Optics. 2009;38(2):124–130. 10.1007/s12596-009-0011-z

[31] Kumawat AK, Rathore SS, Singh S, Nathawat R. Structural transition and photoluminescence behavior of (V2O5)1-x (Ag0.33V2O5)x (x=0 to 0.1) nanocomposites. Results in Chemistry. 2023;5:100802. 10.1016/j.rechem.2023.100802

[32] Bhadra S, Khastgir D, Singha NK, Lee JH. Progress in preparation, processing and applications of polyaniline. Progress in Polymer Science. 2009;34(8):783–810. 10.1016/j.progpolymsci.2009.04.003

[33] Kang M, Chu M, Kim SW, Ryu JW. Optical and electrical properties of V2O5 nanorod films grown using an electron beam. Thin Solid Films. 2013;547:198–201. 10.1016/j.tsf.2013.03.060

[34] Channu VSR, Holze R, Rambabu B, Kalluru RR. Synthesis and characterization of PANI nanostructures for supercapacitors and photoluminescence. Iranian Polymer Journal. 2012;21(7):457–462. 10.1007/s13726-012-0049-7

[35] Ouyang W, Teng F, He J, Fang X. Enhancing the Photoelectric Performance of Photodetectors Based on Metal Oxide Semiconductors by Charge-Carrier Engineering. Advanced Functional Materials. 2019;29(9). 10.1002/adfm.201807672

[36] Zuo G, Ye H, Du J, Ding X. S-scheme Zn-Mn2O4/V2O5 heterojunction for degradation of ciprofloxacin hydrochloride under visible-light irradiation. Journal of Nanoparticle Research. 2025;27(7). 10.1007/s11051-025-06377-0

[37] Mahdi MM, Salim ET, Obaid AS. A Comparison Study of Au@Nb2O5 Core–Shell Nanoparticle Using Two Different Laser Flounces. Plasmonics. 2025;20(8):6313–6326. 10.1007/s11468-024-02746-y

[38] Zhao MX, Chen SR, Hu B, Chen H, Xiao YX, Liu TT, et al. Engineering an Ag2Se@PANi core–shell nanozymes – Klebsiella pasteurii hybrid system with enhanced ammonia synthesis. Bioresource Technology. 2025;427:132436. 10.1016/j.biortech.2025.132436

[39] Shafique S, Yang S, Iqbal T, Cheng B, Wang Y, Sarwar H, et al. Improving the performance of V2O5/rGO hybrid nanocomposites for photodetector applications. Sensors and Actuators A: Physical. 2021;332:113073. 10.1016/j.sna.2021.113073

[40] Baloch AAB, Alharbi FH, Grancini G, Hossain MI, Nazeeruddin MK, Tabet N. Analysis of Photocarrier Dynamics at Interfaces in Perovskite Solar Cells by Time-Resolved Photoluminescence. The Journal of Physical Chemistry C. 2018;122(47):26805–26815. 10.1021/acs.jpcc.8b07069

[41] Nhan DH, Cong HN, Nha NNT, Hai LP, Toan NT, Cuong HL, et al. Annealing-induced oxidation state transition, crystal formation, optical properties, and photocatalytic activity of vanadium oxide nanoparticles. Journal of Nanoparticle Research. 2024;26(5). 10.1007/s11051-024-05994-5

[42] Kumar M, Gour KS, Singh VN. Photodetector performance limitations: Recombination or trapping—Power exponent variation with the applied bias to rescue. Journal of Materials Research. 2023;38(7):1813–1823. 10.1557/s43578-022-00890-x

[43] Chen P, Ma X, Wang Z, Yang N, Luo J, Chen K, et al. Revealing the impact of thermal annealing on the perovskite/organic bulk heterojunction interface in photovoltaic devices. Physical Chemistry Chemical Physics. 2024;26(20):14874–14882. 10.1039/d4cp00849a

[44] Salim ET, Mahdi MM, Obaid AS, Gopinath SCB. Thickness-engineered Au@Nb2O5 thin films for ultrahigh-response photodetectors: Synthesized by pulsed laser in liquid. Optical Materials. 2025;167:117337. 10.1016/j.optmat.2025.117337

[45] Salih EY, Bashir MBA, Rajpar AH, Badruddin IA, Bahmanrokh G. Rapid fabrication of NiO/porous Si film for ultra-violate photodetector: The effect of laser energy. Microelectronic Engineering. 2022;258:111758. 10.1016/j.mee.2022.111758

[46] Salih EY, Sabri MFM, Tan ST, Sulaiman K, Hussein MZ, Said SM, et al. Preparation and characterization of ZnO/ZnAl2O4-mixed metal oxides for dye-sensitized photodetector using Zn/Al-layered double hydroxide as precursor. Journal of Nanoparticle Research. 2019;21(3). 10.1007/s11051-019-4501-x

[47] Lee Y, Yu SH, Jeon J, Kim H, Lee JY, Kim H, et al. Hybrid structures of organic dye and graphene for ultrahigh gain photodetectors. Carbon. 2015;88:165–172. 10.1016/j.carbon.2015.02.071

[48] Meng Z, Zhang T, Zhang C, Shang Y, Lei Q, Chi Q. Advances in Polymer Dielectrics with High Energy Storage Performance by Designing Electric Charge Trap Structures. Advanced Materials. 2023;36(52). 10.1002/adma.202310272

[49] Yang S, Cui X, Gong J, Deng Y. Synthesis of TiO2–polyaniline core–shell nanofibers and their unique UV photoresponse based on different photoconductive mechanisms in oxygen and non-oxygen environments. Chemical Communications. 2013;49(41):4676. 10.1039/c3cc39157d

[50] Rogalski A, Bielecki Z, Mikołajczyk J, Wojtas J. Ultraviolet Photodetectors: From Photocathodes to Low-Dimensional Solids. Sensors. 2023;23(9):4452. 10.3390/s23094452

[51] Bouclé J, Ravirajan P, Nelson J. Hybrid polymer–metal oxide thin films for photovoltaic applications. Journal of Materials Chemistry. 2007;17(30):3141. 10.1039/b706547g

How to cite this article

Ibrahim TA, Obaid AS, Ibraheem IJ. Evaluation the impact of temperature on the photodetection properties of V2O5/PANI nanocomposites. Journal of University of Anbar for Pure Science. 2026; 20(1):222-232. doi:10.37652/juaps.2025.162061.1470